Copyright © 2007 American Scientific Publishers
All rights reserved
Printed in the United States of America

Journal of
Nanoscience and Nanotechnology
Vol. 7, 1–8, 2007

Neutron and X-Ray Scattering on the Monolayer Structure of a Lecithin Fullerene-Derivative

U-Ser Jeng[1,*], Tsang-Lang Lin[2], Kwanwoo Shin[3], Hsin-Yi Lee[1], Chia-Hung Hsu[1], Zau-Ann Chi[4], Ming Chih Shih[4], and Naoya Torikai[5]

[1] *National Synchrotron Radiation Research Center, Hsinchu Science Park, Hsinchu 300, Taiwan*
[2] *Department of Engineering and System Science, National Tsing Hua University, Hsinchu 300, Taiwan*
[3] *Department of Materials Science and Engineering, Gwangju Institute of Science and Technology, Gwangju 500 712, Korea*
[4] *Department of Physics, National Chung-Hsing University, Taichun 410, Taiwan*
[5] *Neutron Science Laboratory, High Energy Accelerator Research Organization, 1-1 OHO, Tsukuba, Ibaraki, 305-0801, Japan*

Using neutron reflectivity with contrast variation, X-ray reflectivity, and grazing incident small-angle X-ray scattering (GISAXS), we have characterized the in-depth and in-plane structural characteristics of the Langmuir and Langmuir-Blodgett (LB) films formed by a novel lecithin C_{60}-derivative, FPTL, of three phospholipids jointly bonded on one single olefinic moiety of a C_{60} cage. Based on the neutron reflectivity measured, we have proposed a monolayer structure, with the C_{60} cages of FPTL lifted into the air and hydrophilic phospholipid heads immersed in water, for the FPTL Langmuir layer formed on water. On the other hand, the LB film of FPTL prepared on mica exhibits clear Kiessig fringes in the X-ray reflectivity profile, indicating a 27 Å monolayer film with less molecular orientation. With GISAXS, we have extracted an in-plane correlation length of about 210 Å for a possible in-plane aggregation of C_{60} of FPTL in the LB monolayer. We have also demonstrated the highly ordered monolayer structures of a lecithin lipid, in elucidating the positive effect of the phospholipids on the monolayer formation of the lecithin C_{60}-derivative.

Keywords: X-Ray and Neutron Reflectivity, Langmuir and Langmuir-Blodgett Film, Lecithin C_{60} Derivative, GISAXS.

RESEARCH ARTICLE

1. INTRODUCTION

Due to the high charge affinity of fullerenes, the embedment of fullerenes or their derivatives into lipid membranes has many interesting consequences, such as high electron transport efficiency of C_{60}-embedded lipid membranes,[1,2] or protection of cells from the attack of reactive oxygen species.[3,4] The efficiency of these effects relates deeply to the aggregation behavior of fullerenes as well as the interactions of the attached functional groups of fullerene derivatives with local environments.[5–7] To avoid the notorious strong self aggregation, thus, a greater fullerene activity, fullerenes are often modified for better water- or lipid-solubility. Structurally, we may roughly classify fullerene derivates into symmetrical and asymmetrical types. For fullerene derivatives of a globular shape, with the hydrophobic center of C_{60} surrounded by symmetrically (or randomly) attached functional groups (for instances, surfactants,[5,8] acids,[9,10] aliphatic chains[11,12]), the many attached functional groups not only significantly consume the olefinic moieties of fullerenes but also block the active fullerene surface. In this case, fullerene-derivatives are dominated by the behavior of the functional groups attached, and the fullerene can be used as a linking center for increasing locally the number density of the functional groups for better mechanical properties or chemical activity of the functional groups.[13]

In another direction of application emphasizing on retaining fullerene activity while improving the compatibility to a specific host, fullerene-derivatives of an asymmetric architecture is preferred: for instance, a rod-like shape[2] with long functional groups attached on one side of a fullerene, or a disk-like shape with the fullerene surrounded by functional groups in an equatorial plane.[4] The asymmetrically attached functional groups are expected to overcome the strong fullerene aggregation by stronger interactions between the functional groups and the functional groups with the environment resided, thus, facilitate the formation of, for instance, a monolayer with more unblocked fullerene surfaces for bio-microsensors or

*Author to whom correspondence should be addressed.

optoelectronic devices.[10, 14] Nevertheless, except for few cases,[15] the formation of compacted monolayers of high density of fullerenes cannot be easily achieved among many amphiphilic C_{60} derivatives[10, 14] although some lipophilic C_{60} derivatives can form bilayers of no water content.[11, 12, 16]

Recently, Chiang et al. in our research group has designed and synthesized an asymmetrical lecithin C_{60} derivative, FPTL, of three phospholipids chemically bonded. The three single-chain phospholipids, mimicking partially the molecular structure of a lecithin lipid dipalmitoylphosphatidylcholine (DPPC), jointly bind on one single olefinic moiety of a C_{60} cage with their aliphatic chains, leaving the three hydrophilic zwitterionic heads (phosphate and choline groups) closely extending out in the same direction (Fig. 1). Compared to the lipophilic C_{60} derivatives reported, on the basis of attaching hydrophobic aliphatic chains to a fullerene for globular structure[11, 12] or rod-like shape,[17, 18] the FPTL studied here is unique in the attached phospholipids containing the lipophilic aliphatic chains as well as hydrophilic zwitterionic heads. With the three phospholipids, FPTL can form monolayers on water surface or mica substrate, as revealed by neutron and X-ray reflectivity to be detailed below. On the other hand, with the three phospholipids, FPTL can also be intercalated into vesicles of DPPC in an aqueous solution for forming a strengthened membrane complex of higher bending elasticity.[13]

Despite neutron and X-ray reflectivity has been regularly adopted in extracting in-depth structural information of films of fullerene derivatives,[19, 20] the study of in-plane aggregation structures of C_{60}-derivative monolayers is very seldom reported. In-plane scattering for the in-plane structure of an organic monolayer demands a high flux of X-ray or neutron due to the very low scattering sample volume and scattering intensity. Technically, a good alignment of the monolayer film to the incident beam ~~for~~ an optimized incident angle (usually ~0.2° for Si or glass substrate) is also critical in conducting in-plane scattering. With grazing incident small-angle X-ray scattering (GISAXS) based on a synchrotron radiation X-ray source,[21] we have explored the possible in-plane aggregation of the lecithin C_{60} derivative in ~~a~~ LB film. To elucidate the benefit of the attached phospholipid, especially the zwitterionic heads, of FPTL in facilitating the monolayer formation, we ~~have measured and~~ present the highly ordered monolayer structures of the pure phospholipid DPPC.

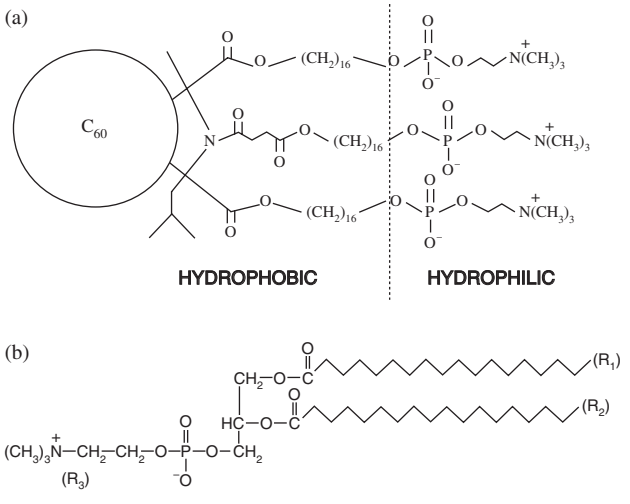

Fig. 1. Schematics of the molecular structures of the lecithin C_{60}-derivative, FPTL (a), and the lecithin lipid DPPC (b).

2. EXPERIMENTAL DETAILS

2.1. Materials and Sample Preparation

Figure 1 illustrates the schematic views of DPPC and the novel lecithin C_{60} derivative, FPTL, having three phospholipid chains chemically bonded on one olefinic moiety of the C_{60} cage. With the C_{60} cage and the aliphatic chains representing the hydrophobic end and the phosphate and choline groups for the hydrophilic end, the linear or rod-like FPTL has a fully stretched length ≈39 Å, which is larger than the 29 Å of DPPC mainly by the additional C_{60} cage of a dia. ≈10 Å. The detailed synthesis route for FPTL, having a molecular weight M_w of 2178 g/mol, will be reported elsewhere. After synthesis, FPTL was stored in a co-solvent of dichlorobenzene and DMSO (3 : 2) with a concentration of 4 mg/ml. In preparing a sample solution for spreading Langmuir monolayers on water, a small amount of FPTL solution was vacuum-dried in a glass tube (resulting in a uniform FPTL thin film on the glass wall), and the sample was re-dissolved by the co-solvent of benzene and chloroform (2 : 1 in volume ratio). The result FPTL solution, of a nominal concentration of 0.625 mg/ml, was brownish and isotropic; there was, however, sedimentation due to a limited solubility. A sample solution of DPPC (1,2-Dipalmitoyl-sn-glycero-3-phosphocholine, $M_w = 734$ g/mol), of a concentration of 5.6 mg/ml in chloroform, was also prepared. The ~~LB~~ films of FPTL and DPPC were transferred, respectively, onto mica substrates (of an area of 6.5×2.5 cm^2 at a constant surface pressure of 26 and 30 mN/m at 20 °C, ~~respectively~~, using vertical dipping method with a dipping speed of 25 mm/min. The large pressures used in transferring the ~~LB~~ films were to obtain compact monolayers.

2.2. Measurements

The pressure–area (π–A) isotherms for the samples were observed with a typical compression speed of 80 cm^2/min on a NIMA Langmuir trough of an area of 500 cm^2 at 20 °C. A different compression speed of 10 cm^2/min was also tried, and the result isotherms showed little dependence on the two compression speeds.

Neutron reflectivity measurements for FPTL and DPPC Langmuir films at the air-water interface were conducted (at 23 °C) on the NG7 neutron reflectometer quipped

with a Langmuir trough, at the National Institute of Standards and Technology (NIST), USA.[22] In the reflectivity scans with neutrons of a wavelength of 4.77 Å, the beam width was fixed to 25 mm, whereas the beam height was increased stepwise from 0.1 to 4 mm as Q moved from 0.01 to 0.2 Å^{-1} for keeping a constant Q resolution. Here, the wavevector transfer perpendicular to the sample surface, $Q = 4\pi \sin\theta/\lambda$, is defined by the scattering angle 2θ and the wavelength λ of neutrons. With D_2O and H_2O for scattering contrast variation of subphase, two sets of reflectivity profiles can be obtained for a common monolayer structure. The contrast variation method gives a strong constraint in extracting the structure of a monolayer from reflectivity data.[23] For a wider Q range up to 0.3 Å^{-1} the ARISA neutron reflectometer for liquid surfaces at a pulsed neutron source of KENS, KEK, detailed previously,[24, 25] was also adopted in the DPPC-d_{62}/D_2O system, where d_{62} denotes the replacement of the 62 hydrogen atoms in the aliphatic chains of DPPC by deuterons, D, for enhancing (or highlighting) neutron scattering from the chains.

X-ray reflectivity and GISAXS for the LB films were conducted on a setup based on an 8-circle diffractometer of the wiggler beamline BL17B at the National Synchrotron Radiation Research Center (NSRRC) of Taiwan. The beam was monochromated to $\lambda = 1.55$ Å by a double crystal monochromator (DCM) of Si(111), and collimated by two sets of slits (0.4×0.4 mm^2 and 0.4×0.6 mm^2) separated by one meter. The result photon flux at the sample position was $\sim 10^9$ photons/s. With the mechanics of the 8-circle diffractometer, we could position and align samples and detectors for in-plane GISAXS as well as reflectivity measurements. A scintillation counter or a position sensitive linear detector was selectively mounted at the position $\sim$1 m from the sample for reflectivity or GISAXS measurement. The GISAXS setup gave an angular resolution of 0.028° and 0.006°, or a Q-resolution of 0.004 Å^{-1} and 0.001 Å^{-1}, in the vertical and horizontal directions, respectively. And the minimum instrumental Q value achieved, $\sim$0.01 Å^{-1}, allows a structural characterization for systems of aggregation sizes up to several hundreds angstroms.[21] For all the GISAXS measurements, the incident angle was fixed at 0.225°, or $Q_z = 0.033$ Å^{-1}, which was slightly larger than the critical angle for total reflection of mica. The GISAXS data were collected along the in-plane direction, where the wavevector transfer parallel to the sample surface $Q_{xy} = 4\pi \sin\theta_{xy}/\lambda$ was defined by the in-plane scattering angle $2\theta_{xy}$ and λ.

3. RESULTS AND DISCUSSION

3.1. Isotherms

The π–A isotherm measured for FPTL at 20 °C (Fig. 2) is characterized by the slow-varying pressure across a wide range of molecular area. Furthermore, the isotherm

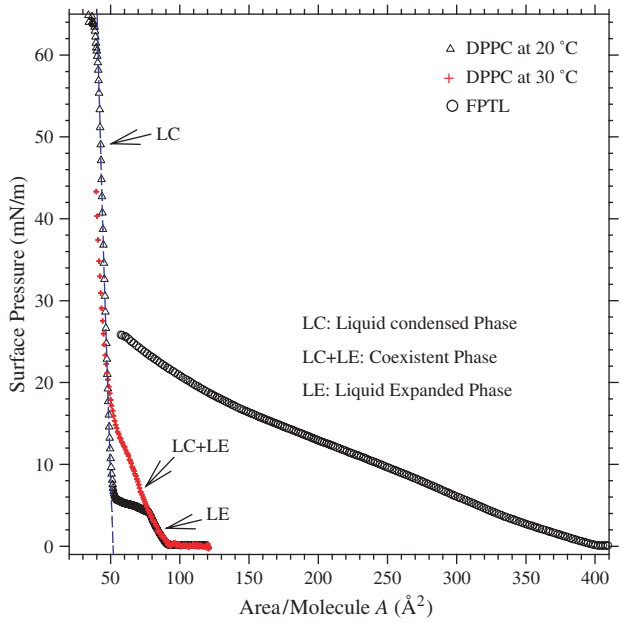

Fig. 2. π–A isotherms for FPTL and DPPC measured on H_2O subphase. The arrows indicate the liquid expanded phase LE, the coexistent phase (LE+LC), and the liquid condensed phase LC, for DPPC at 20 °C. The dashed line extrapolates a limiting area per molecule of 50 Å^2 for DPPC. Note, the scale of A is only for the DPPC isotherm, but not for the FPTL isotherm, due to an incomplete dissolving of FPTL in the sample solution (see text).

observed for FPTL is reversible, provided that π is kept under 16 mN/m. The reversibility, the lacking of low-compressibility region, and the large compressibility exhibited in the isotherm observed, together indicate a liquid-like molecular organization for the FPTL film of long-range in-plane interactions, resulted from the balance between the attraction of fullerenes and the repulsion of zwitterionic heads. On the other hand, the FPTL π–A isotherm differs from that for DPPC at 20 °C (Fig. 2) where the three characteristic regions—the liquid expand (LE), the liquid condensed (LC), and the coexistent (LE+LC) phases, of DPPC—can be clearly identified.[26] At higher temperatures (Fig. 2), FPTL and DPPC, nevertheless, have closer isotherm features. Likely, the coexistent phase of well-packed chains of DPPC deteriorates due to larger thermal fluctuations, and the isotherm is dominated more by the lipid headgroups as is the case of FPTL. From these results, it is possible that, limited by the structure, the three lecithin chains attached to the same olefinic moiety of the C_{60} cage of FPTL cannot orientate or stretch freely for a good chain-packing as the pure DPPC does at the same temperature (20 °C) during the film compression. Since the phosphate group and the choline group of the phospholipid, tend to stick together and occupy an area of $\sim$50 Å^2 on the water surface (extrapolated from the isotherm of DPPC in Fig. 2), the three neighboring phospholipid heads of FPTL, covering an area close to 150 Å^2, presumably can also provide an anchoring for FPTL on the water surface for forming monolayers. This mechanism

RESEARCH ARTICLE

of Langmuir monolayer formation of FPTL differs fundamentally from that reported for lipophilic fullerene derivatives of only hydrophobic aliphatic chains.[15]

The lacking of low compressibility region in the FPTL isotherm observed indicates that the area per FPTL may be larger than the limiting area A_o of a fullerene (87 Å^2 measured by Hernandez et al.[27] or 96 Å^2 by Obeng et al.),[28] in the compression region. Nevertheless, the less-reversible isotherm with $\pi > 16$ mN/m suggests that FPTL molecules may form non-reversible in-plane attachment when they are close enough, due to the strong attraction between fullerenes.

3.2. Neutron Reflectivity for Monolayer Structures

Figure 3 shows the neutron reflectivity data for the FPTL films compressed to a surface pressure of $\pi = 14$ mN/m, on D_2O and H_2O, respectively. Such a surface pressure likely corresponds to a monolayer film of FPTL, based on the isotherm result shown previously. Compared to the data of pure H_2O subphase, the higher reflectivity for the FPTL/H_2O surface indicates the existence of an FPTL layer on water, due mainly to the higher scattering length density, ρb, of C_{60} cage than the H_2O subphase.[29] Compared to the fullerenes, the phospholipids of FPTL contribute less to the reflectivity profile, as can be seen from the lower reflectivity profile of the DPPC monolayer of a high packing density on H_2O (Fig. 5). The reflection effect of the phospholipids of FPTL can be enhanced by the replacement of H_2O subphase with D_2O, due to the hydration effect of the phospholipid heads of FPTL. As shown in Figure 3, the reflectivity data measured for the FPTL film on D_2O surface gradually fall below that for pure D_2O as Q increases, which reflects the scattering effect from the hydration layer, of a lower ρb value, on D_2O surface.

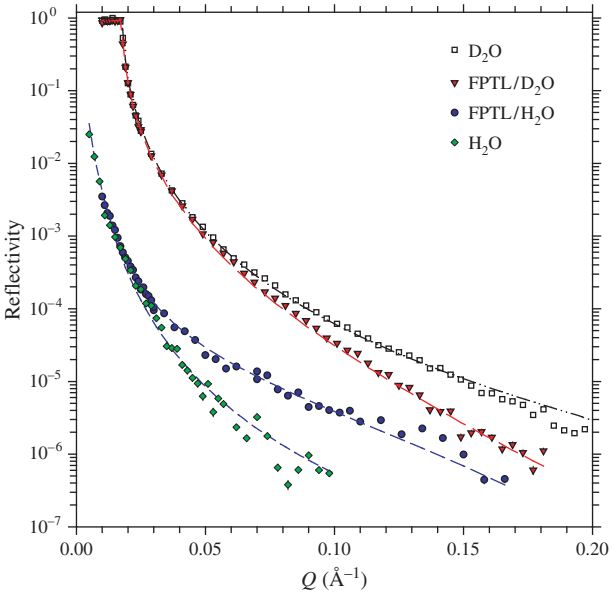

Fig. 3. Neutron reflectivity data collected for the FPTL Langmuir films on D_2O and H_2O, respectively. The data are fitted (dashed curves) using the scattering length density profiles shown in Figure 4. For a comparison, the reflectivity data and the corresponding simulations for D_2O and H_2O are also shown.

It is difficult to extract a detailed structure for the thin FPTL monolayer film of a small thickness, ~30 Å, using a single reflectivity profile limited in a relatively short Q-range (compared the X-ray data shown below).[30] Nevertheless, with the contrast provided by the two reflectivity profiles, the characteristics of the Langmuir film of FPTL can be identified. Furthermore, the two sets of contrast data together place a strong constraint in the data fitting for extracting a detail structure of the FPTL monolayer. After numerous trials in data fitting using a model fitting algorithm for multilayer structures,[31] we have settled with a three-layer model for the ρb profile of the FPTL Langmuir layer, which can account for the two sets of contrast reflectivity data harmonically (dashed curves in Fig. 3). In the fitting algorithm, the continuous transition between successive layers of different ρb values is accounted by an interfacial width w.[31] Table I lists the fitted structural parameters ρb, w, and the layer thickness d for the three layers.

Based on the two ρb profiles obtained for FPTL on D_2O and H_2O (Fig. 4), we have proposed a structural model for the FPTL monolayer on water as shown in Figure 4. In the model, we respectively attribute the first and second layers, L1 and L2, to the C_{60}-rich and aliphatic chain-rich layers above water surface. Whereas the third layer L3 of a ρb value strongly influenced by D_2O or H_2O represents the

Table I. Parameters for the scattering length density, ρb, profiles used to simulate the neutron reflectivity data of FPTL and DPPC Langmuir layers on D_2O and H_2O, with d for the thickness of each sublayer and w for the interfacial width between sublayers. The molecular area A and the hydration number n are calculated from the parameters in the hydration layers (sublayer 3). Symbol $w = 2(2)^{1/2}\sigma$, where σ is the root-mean-squared roughness.

	Sublayers	ρb (10^{-6} Å^{-2})	d (Å)	w (Å)	A (Å^2)	n
FPTL/H_2O	Sublayer 1	1.00	7	4		
($\pi = 14$ mN/m)	Sublayer 2	0.70	7	4		
	Sublayer 3	0.10	13	4		
	Subphase (H_2O)	−0.56	—	4		
FPTL/D_2O	Sublayer 1	1.00	7	4		
($\pi = 14$ mN/m)	Sublayer 2	0.70	7	4		
	Sublayer 3	4.80	13	4	200	72
	Subphase (D_2O)	6.36	—	4		
DPPC-d_{62}/D_2O	Sublayer 1	6.45	16	8		
($\pi = 16$ mN/m)	Sublayer 2	3.55	10	4	49	8
	Subphase (D_2O)	6.36	—	4		
DPPC/H_2O	Sublayer 1	−0.3	16	8		
($\pi = 50$ mN/m)	Sublayer 2	1.15	9	4		
	Subphase (H_2O)	−0.56	—	4		
DPPC/D_2O	Sublayer 1	−0.3	16	8		
($\pi = 20$ mN/m)	Sublayer 2	3.60	12	3	43	9
	Subphase (D_2O)	6.36	—	3		

RESEARCH ARTICLE

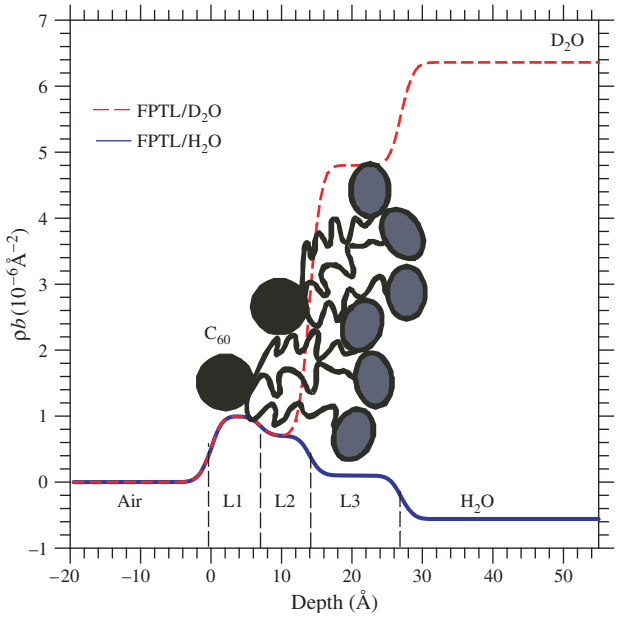

Fig. 4. Scattering length density profiles used to simulate the reflectivity data in Figure 3. The cartoon illustrates the FPTL monolayer structure on water, characterized by the L1, L2, and L3 sublayers of the ρb profiles.

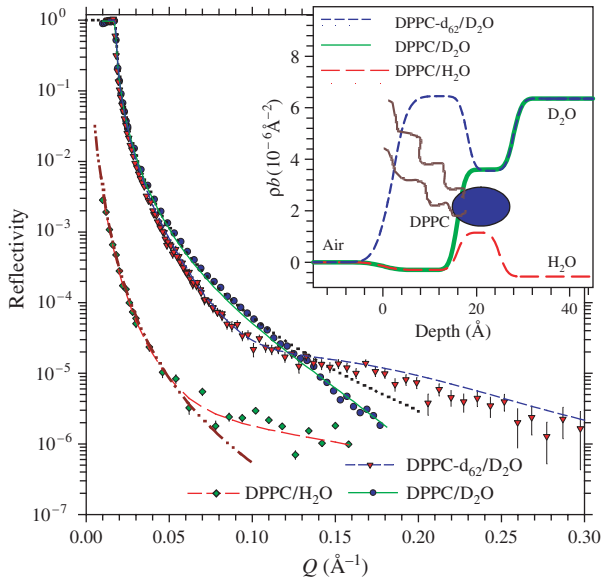

Fig. 5. Neutron reflectivity data collected for the compressed DPPC monolayers on water, including DPPC/D_2O at $\pi = 20$ mN/m, DPPC-d_{62}/D_2O at $\pi = 16$ mN/m, and DPPC/H_2O at $\pi = 50$ mN/m. The three sets of data are fitted, respectively using the ρb profiles shown in the inset. The simulated reflectivity profiles for D_2O (dotted curve) and H_2O (dot-dashed curve) are also shown for comparison. The cartoon in the inset illustrates the orientation of DPPC on water for the hydrophobic and hydrophilic sublayers.

hydration layer of the phospholipid heads of FPTL. The structural model for the FPTL Langmuir monolayer differs fundamentally from that given by Mouri et al.[15] for a lipophilic fullerene. In their model, the aliphatic chains of the lipophilic C_{60} derivative studied were brought up into air, left fullerenes in contact with water. The differences between the two models illustrate the effect of hydrophilic heads of FPTL in the monolayer formation.

From the fitted ρb value, 4.8×10^{-6} Å^{-2}, for the hydration layer of FPTL on D_2O (see Table I), we obtain a molecular area $A = 200$ Å^2 for FPTL using $(\rho b) - (\rho b)_w = [b_h - V_h(\rho b)_w]/(Ad)$.[30,32] Here, $(\rho b)_w$ and d are respectively the scattering length density of water (D_2O) and the thickness of the hydration layer (with the transition zone thickness taken into account).[33] Whereas $b_h (= 468.5 \times 10^{-6}$ Å) and $V_h (= 335$ Å^3) are the scattering length and dry volume for each phospholipid head of FPTL.[34,35] The molecular area $A = 200$ Å^2 obtained for FPTL is roughly two times larger than the cross section of C_{60}, implying a ~~not~~ overlapped dispersion of C_{60} cages in the FPTL monolayer. A hydration number $n = 72$ (number of water molecules associated with the hydrophilic heads of FPTL) is also deduced from $Ad = nV_w + V_h$ with the structural parameters for the hydration layer shown in Table I. Here $V_w = 30.3$ Å^3 is the volume of a water molecule.[32]

To elucidate the effect of the phospholipid heads in forming Langmuir monolayers, we have measured the neutron reflectivity data for pure DPPC monolayers compressed to the liquid condensed phase. Figure 5 shows the three sets of reflectivity data taken for the DPPC-d_{62} on D_2O at $\pi =$ 16 mN/m, DPPC on D_2O at $\pi = 20$ mN/m, and DPPC on H_2O at $\pi \sim 50$ mN/m. Despite the significant differences in the pressures, the three DPPC monolayer structures in the same liquid condensed phase should be similar.[36] Indeed, the three ρb profiles fitted (inset in Fig. 5) correspond to a common two-layer structure, namely, a layer of aliphatic chains on top of a hydration layer of phospholipid heads. The detailed parameters fitted for each set of data are summarized in Table I. The well-defined two-layer structure obtained indicates ordered DPPC monolayers on water surface. From the structural parameters for the DPPC/D_2O system, we can extract a dry volume of DPPC $V = 1275 \pm 100$ Å^3 (added from the volumes 335 Å^3 of the hydrophilic head and 940 ± 100 Å^3 of the two disordered aliphatic chains), with a molecular area $A = 49$ Å^2 and a hydration number of ~~4~~. These values are consistent with that given by Koenig et al.[34] and Vaknin et al.[35]

3.3. X-Ray Reflectivity for the LB Films

Figure 6 shows the X-ray reflectivity data for the FPTL LB film transferred to mica substrate at $\pi = 26$ mN/m. The critical Q for total reflection (Reflectivity = 1) measured for the FPTL film is mainly contributed by the mica substrate, as compared to the reflectivity profile measured for a pure mica substrate (Fig. 6). Furthermore, the period of the Kiessig fringes observed in the reflectivity profile indicates a film thickness of ~27 Å for the FPTL monolayer. Using the same fitting algorithm as that used for neutron reflectivity analysis, we can fit the X-ray data of the FPTL LB film well using a single layer model

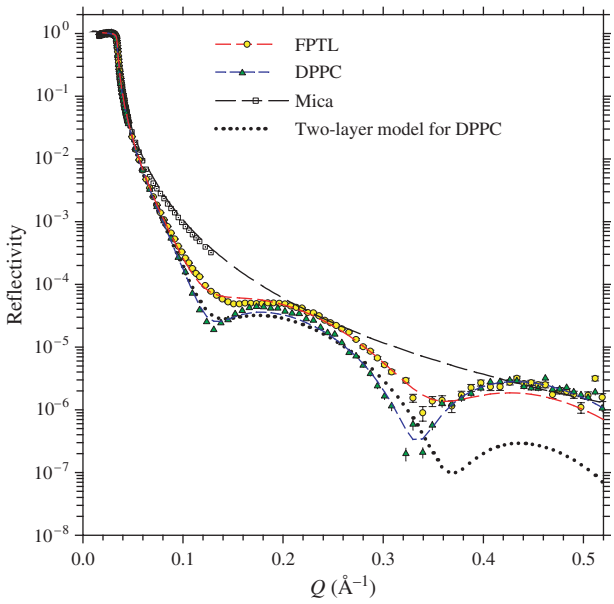

Fig. 6. X-ray reflectivity data for the FPTL and DPPC LB films are fitted (dashed curves) using the corresponding ρb profiles shown in Figure 7. The dotted curve is a simulation for the DPPC data using a two-layer model (hydrophobic and hydrophilic sublayers) for the ρb profile. Also shown are the data for mica substrate and the corresponding simulation (long dashed curve).

(Fig. 7) with a film thickness $d = 27 \pm 2$ Å and a ρb value of 7.0×10^{-6} Å^{-2}. From the structural parameters fitted (summarized in Table II), we deduce $A = 180 \pm 10$ Å^2 for FPTL in the LB film, using the same method as we have done previously for the FTPL Langmuir film at the

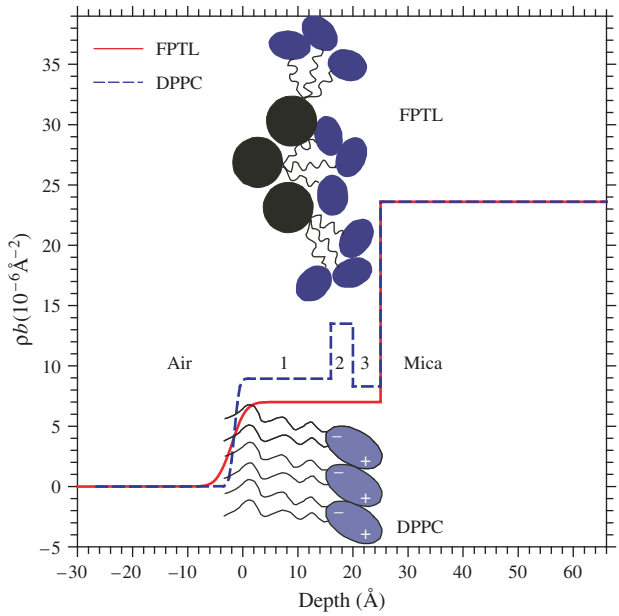

Fig. 7. ρb profiles used in fitting the reflectivity data in Figure 6. The cartoons illustrate the monolayer structures of the FPTL and DPPC LB films, on the basis of the ρb profiles fitted. The numbers 1, 2, and 3, represent the three sublayers of the aliphatic chains, the PO_4^{-1} groups, and the choline groups in the DPPC LB film.

Table II. Parameters for the ρb profiles used to simulate the X-ray reflectivity data of the FPTL and DPPC LB films, with d for the sublayer thickness, w the interfacial width, and A the area/molecule.

	Index of Layer	ρb (10^{-6} Å^{-2})	d (Å)	w (Å)	A (Å^2)
FPTL/mica	FPTL	7.0	27	6	180
	Mica substrate	23.6	—	0	
DPPC/mica	Sublayer 1 (Chains)	8.95	17.5	2	43
	Sublayer 2 (PO_4^{-1})	13.5	4	0	
	Sublayer 3 (Choline)	8.3	5	0	
	Mica Substrate	23.6	—	—	

air–water interface, but with $(\rho b)_w$ replaced by $(\rho b)_{air} = 0$ for the case of LB film. The smaller film thickness of 27 Å (implying a tilt of ~50° of FPTL from the film normal, when compared to the fully stretched length 38 Å of FTPL) together with the larger molecular area $A = 180$ Å^2 (compared to the limiting area ~90 Å^2 of a fullerene or the area of ~150 Å^2 for the three zwitterinoic heads of FPTL estimated from Table I), indicates a monolayer film of FPTL with less in-plane ordering than the DPPC LB film.

The X-ray reflectivity profile measured for the DPPC LB film on mica (Fig. 6) demonstrates sharp Kiessig fringes ~~of a film of sharp interfaces~~. The film thickness extracted from the period of the Kiessig fringes is 27 Å, matching well the single DPPC molecular size. In fitting the data for a detailed film structure, we ~~realize~~ that the straightforward two-layer ρb model used previously for the Langmuir monolayer of DPPC, consisting of a hydrophilic layer of phospholipid heads and a hydrophobic layer of aliphatic chains, can only account for the reflectivity features in the Q range within 0.3 Å^{-1} (dotted curve in Fig. 6). To describe the full range of data up to $Q \sim 0.5$ Å^{-1}, we have to use a three-layer model, in which the hydrophilic layer is further decomposed into two sublayers of the phosphate group PO_4^- and the choline group. A similar structural model was also mentioned by Schalke et al. recently.[30] With the three-layer model for the ρb profile, we can well simulate (dashed curve in Fig. 6) the whole reflectivity data of the DPPC LB film. Figure 7 shows the best-fitted ρb profile, of a total film thickness of ~ 27 Å contributed by the three sublayers L1, L2, and L3, corresponding respectively to the aliphatic chains, the phosphate group (of a high electron density), and the choline group. The detailed structural parameters of the ρb profile fitted are summarized in Table II. From the fitted parameters, we can deduce mean molecular area $A = 43$ Å^2 and a volume $V = 1213$ Å^3 for the DPPC in the LB film, as that have been done previously. These values are consistent with that obtained for the DPPC Langmuir film on D_2O.[34, 35] We attribute the highly aligned DPPC to the consequence of charge interactions between the electric dipoles of the zwitterionic heads and the mica of a negative

RESEARCH ARTICLE

charge surface,[37, 38] as illustrated by a cartoon in Figure 7. On the other hand, in the X-ray reflectivity measurement for a DPPC LB film sealed in a high humidly environment (data not shown), we have also observed a deteriorated ordering of the LB film structure as the humidity increased from 50% to ~90%. The result suggests that dehydration of the LB transferred lipid monolayer also contributes significantly to the high alignment of DPPC in the LB film. In contrast, even in the liquid condensed phase the alignment of DPPC in a Langmuir monolayer will not be easy due to the still present diffusion of molecules within the plane of the monolayer.

3.4. GISAXS for In-Plane Structure

In Figure 8, we show the GISAXS result for the two LB films of FPTL and DPPC. In the case of DPPC, there is little in-plane scattering intensity from the LB film, as compared to the scattering from a pure mica substrate of homogeneous density. This result is consistent with the conclusion from the X-ray reflectivity analysis. Specifically, to exhibit the characteristic of clearly separated sublayers (functional groups) across the film, the aliphatic chains, phosphate, and choline groups of the DPPC molecules must have excellent individual alignment along the in-plane direction, leading to a homogeneous density distribution in the direction, thus, little in-plane scattering.

In contrast, the prominent GISAXS intensity for the FPTL film indicates an inhomogeneous density distribution in the in-plane direction. Using the Debye-Buche

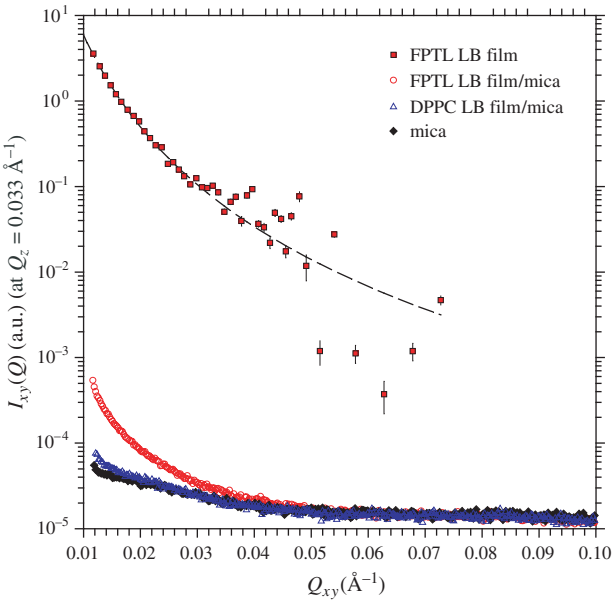

Fig. 8. GISAXS data for the FPTL and DPPC LB films on mica, collected at an incident angle of 0.225° (corresponding to $Q_z = 0.033$ Å^{-1}). Also shown are the GISAXS data for the mica substrate. The net GISAXS profile for the FPTL film, with the scattering contribution from mica substrate subtracted, is fitted with the Debye-Bueche model (dashed curve).

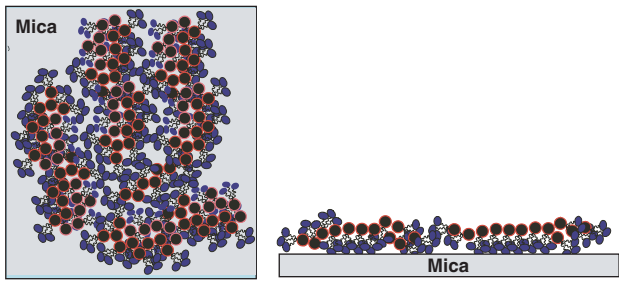

Fig. 9. Cartoons for the top view and side view of the LB film of FPTL on mica, illustrating exaggeratedly the in-plane fullerene (circled disks) aggregation.

model,[7] we fit the in-plane scattering profile with $I(Q_{xy}) \propto (1 + Q_{xy}^2 \xi^2)^{-2}$ (dashed curve in Fig. 8), and extract a correlation length $\xi = 210 \pm 10$ Å for the FPTL film. We attribute the in-plane correlation to a possible aggregation of C_{60} cages of a relatively high charge density (~0.69 e$^-$/Å^3), compare to the phospholipids of FPTL in the film. Considering the structural restrictions placed by the three phospholipids attached to each fullerene and the small film thickness observed in the reflectivity measurement, we suspect that the fullerenes of FPTL most likely form only two-dimensional aggregation of a size of roughly 2ξ in the LB film,[39] as naively proposed in Figure 9.

4. CONCLUSIONS

We have used π–A isotherm, neutron reflectivity with contrast variation, X-ray reflectivity, and GISAXS to characterize the monolayer structures of the Langmuir and LB films formed by the novel lecithin C_{60}-derivative FPTL. All features observed for the monolayer structures of FPTL indicate that the three phospholipids jointly bonded on one single olefinic moiety of the C_{60} cage can facilitate the lecithin C_{60}-derivative in forming Langmuir monolayers on water or LB monolayers on mica. The highly ordered DPPC monolayers on water and mica substrates observed clearly demonstrate the benefit of using lecithin lipids as functional groups in synthesizing C_{60} derivative for monolayer formation. The success in forming FPTL monolayers may have implications in the design of new class of lecithin C_{60}-derivatives for bio-sensors or substrates that can be used in imaging biological macromolecules with scanning electrochemical microscopy.[40]

Acknowledgments: We thank Dr. L. Y. Chiang for providing the sample, and acknowledge the supports of the National Institute of Standards and Technology (NIST) for the use of the NG7 neutron reflectometer and the KENS, KEK, for the ARISA neutron reflectometer. The critical comments from one of the reviewers are appreciated. This work was supported partly by the National Science Council, grant NSC 93-2112-M-213-011 (U. Jeng) and NSC 91-2113-M-007-037 (T.-L. Lin).

RESEARCH ARTICLE

References and Notes

1. C. H. Kuo and D. Mauzerall, *Nature* 361, 138 **(1993)**.
2. N. Nakashima, Y. Yamaguchi, H. Eda, M. Kunitake, and O. Manabe, *J. Phys. Chem. B* 101, 215 **(1997)**.
3. I. Szymanska, H. Radecka, J. Radecki, and D. Kikut-Ligaj, *Biosens. Bioelectron.* 16, 911 **(2001)**.
4. I.-C. Wang, L. A. Tai, D. D. Lee, P. P. Kanakamma, C. K.-F. Shen, T.-Y. Luh, C. H. Cheng, and K. C. Hwang, *J. Med. Chem.* 42, 4614 **(1999)**.
5. U. Jeng, T.-L. Lin, T.-S. Chang, H.-Y. Lee, C.-H. Hsu, Y.-W. Shieh, T. Canteenwala, and L. Y. Chiang, *Progress in Colloid and Polymer Sci.* 118, 232 **(2001)**.
6. S. Niu and D. Mauzerall, *J. Am. Chem. Soc.* 24, 5791 **(1996)**.
7. U. Jeng, T.-L. Lin, K. Shin, C.-H. Hsu, H.-Y. Lee, M. H. Wu, Z. A. Chi, M. C. Shih, and L. Y. Chiang, *Physica B* 336, 204 **(2003)**.
8. W. Zhang, Y. Shi, L. Gan, N. Wu, C. Huang, and D. Wu, *Langmuir* 15, 6921 **(1999)**.
9. D. Vaknin, *Physica B* 221, 152 **(1996)**.
10. J.-L. Gallani, D. Felder, D. Guillon, B. Heinrich, and J.-F. Nierengarten, *Langmuir* 18, 2908 **(2002)**.
11. M. Brettreich, S. Burghardt, C. Bottcher, T. Bayerl and A. Hirsch, *Angew. Chem. Int. Ed.* 39, 1845 **(2000)**.
12. M. Hetzer, T. Gutberlet, M. F. Brown, X. Camps, O. Vostrowsky, H. Schonberger, H. Hirsch, and T. M. Bayerl, *J. Phys. Chem. A* 103, 637 **(1999)**.
13. L. Y. Chiang and L. Y. Wang, *TRIP* 4, 298 **(1996)**.
14. J.-F. Nierengarten, J.-F. Eckert, Y. Rio, M. P. Carreon, J. L. Gallani, and D. Guillon, *J. Am. Chem. Soc.* 123, 9743 **(2001)**.
15. E. Mouri, T. Nakanishi, N. Nakashima, and H. Matsuoka, *Langmuir* 18, 10042 **(2002)**.
16. T. Nakanishi, M. Morita, H. Murakami, T. Sagara, and N. Nakashima, *Chem. Eur. J.* 8, 1641 **(2002)**.
17. H. Murakami, Y. Watanabe, and N. Nakashima, *J. Am. Chem. Soc.* 118, 4484 **(1996)**.
18. M. Matsumoto, H. Tachibana, R. Azumi, M. Tanaka, G. Yunome, M. Abe, S. Yamago, and E. Nakamura, *Langmuir* 11, 660 **(1995)**.
19. A. P. Maierhofer, M. Brettreich, S. Burghardt, O. Vostrowsky, A. Hirsch, S. Langridge, and T. M. Bayerl, *Langmuir* 16, 8884 **(2000)**.
20. S. Burghardt, A. Hirsch, N. Medard, R. A. Kachfhe, D. Aussere, M. P. Valignat and J. L. Gallani, *Langmuir* 21, 7540 **(2005)**.
21. C.-H. Hsu, U. Jeng, H.-Y. Lee, D. Windover, T.-M. Lu, and C. Jin, *Thin Solid Films* 472, 323 **(2004)**.
22. A. Karim, J. F. Douglas, F. Horkay, L. J. Fetters, and S. K. Satija, *Physica B* 221, 331 **(1996)**.
23. S. Krueger, C. W. Meuse, C. F. Marjkrzak, J. A. Dura, N. F. Berk, M. Tarek, and A. L. Plant, *Langmuir* 17, 511 **(2001)**.
24. E. Mouri, K. Matsumoto, H. Matsuoka, and N. Torikai, *Langmuir* 21, 1840 **(2005)**.
25. N. Torikai, M. Furusaka, H. Matsuoka, Y. Matsushita, M. Shibayama, A. Takahara, M. Takeda, S. Tasaki, and H. Yamaoka, *Appl. Phys. A* 74 [Suppl.], S264 **(2002)**.
26. N. Krasteva, D. Vollhardt, G. Brezesinki, and H. Mohwald, *Langmuir* 17, 1209 **(2001)**.
27. M.-P. Hernandez, F. Monroy, F. Ortega, R. G. Rubio, *Langmuir* 17, 3317 **(2001)**.
28. Y. S. Obeng and A. J. Bard, *J. Am. Chem. Soc.* 113, 6279 **(1991)**.
29. M. Fukuto, K. Penanen, R. K. Heilmann, P. Pershan, and D. Vaknin, *J. Chem. Phys.* 107, 5531 **(1997)**.
30. M. Schalke and M. Losche, *Adv. Coll. Inter. Sci.* 88, 243 **(2000)**.
31. J. F. Ankner and C. F Majkrzak, Neutron Optical Devices and Applications, edited by C. F. Majkrzak and J. L. Woods, *Proc. SPIE 1738* **(1992)**, p. 260.
32. W.-J. Liu, U. Jeng, T.-L. Lin, S. H. Lai, M. C. Shih, C.-S. Tsao, L. Y. Wang, L. Y. Chiang, and L. P. Sung, *Physica B* 283, 49 **(2000)**.
33. U. Jeng, L. Esibov, L. Crow, S. S. Malik, and A. Steyerl, *J. Phys.: Condens. Matter* 10, 4955 **(1998)**.
34. B. W. Koenig, S. Krueger, W. J. Orts, C. F. Majkrzak, N. F. Berk, J. V. Silverton, and K. Gawrisch, *Langmuir* 12, 1343 **(1996)**.
35. D. Vaknin, K. Kjaer, J. Als-Nielsen, and M. Losche, *Biophys. J.* 59, 1325 **(1991)**.
36. C. Naumann, T. Brumm, A. R. Rennie, J. Penfold, and T. M. Bayerl, *Langmuir* 11, 3948 **(1995)**.
37. A. G. Wu, Z. Li, L. H. Yu, H. D. Wang, and E. K. Wang, *Anal. Sci.* 17, 583 **(2001)**.
38. P. Skurski, J. Rak, J. Simons, and M. Gutowski, *J. Am. Chem. Soc.* 123, 11073 **(2001)**.
39. U. Jeng, W.-J. Liu, T.-L. Lin, L. Y. Wang, and L. Y. Chiang, *Fullerene Sci. Technol.* 7, 599 **(1999)**.
40. F.-R. Fan and A. J. Bard, *PANS* 96, 14222 **(1999)**.

Received: 8 February 2006. Revised/Accepted: 13 June 2006.